Carnegie stage 4: Attaching blastocyst
5-6 days after fertilization, 0.1-0.2 mm in diameter

This stage is characterized by the attached blastocyst, which corresponds to the onset of implantation. Attachment of the embryo occurs only once the endometrium has entered the secretory phase. At the site of attachment, the trophoblast cells are transformed into a

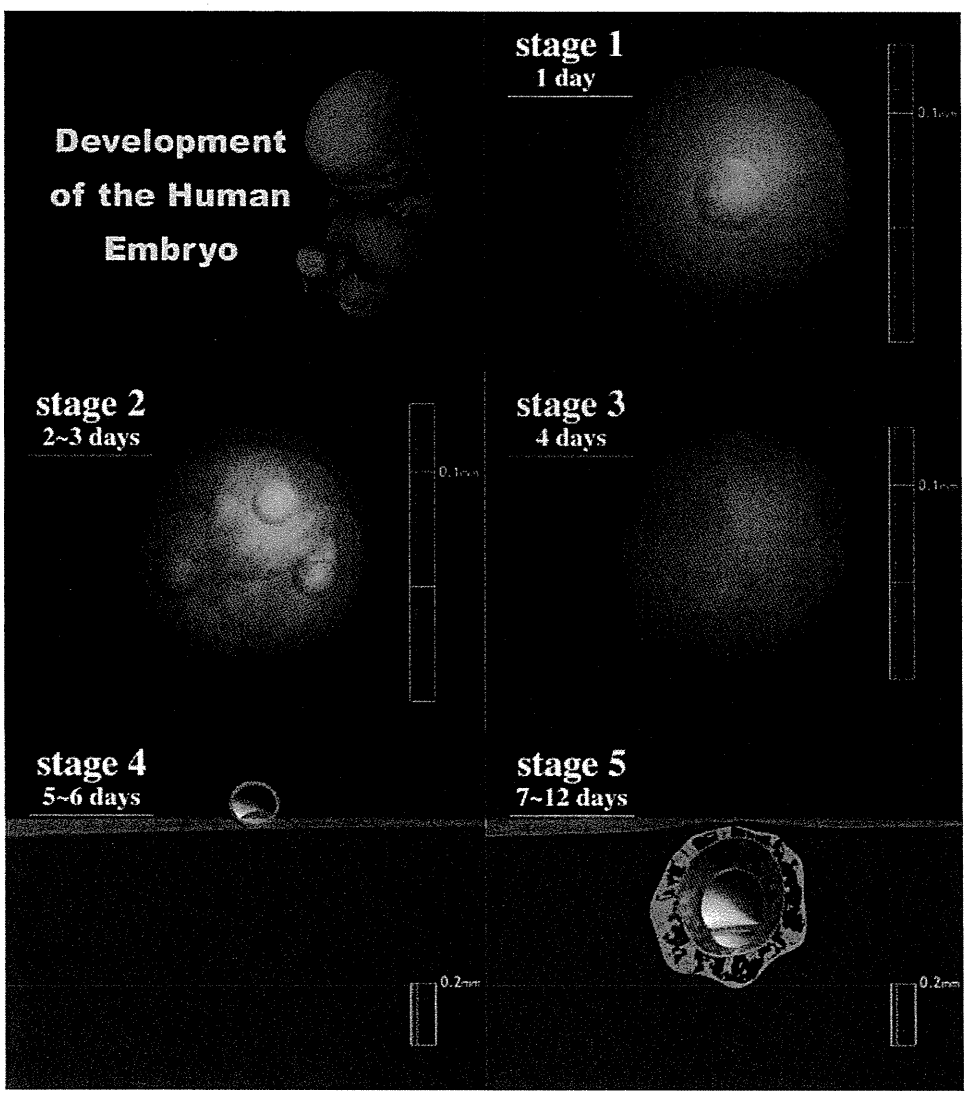

Fig. 3. Computer graphics illustrating embryonic human development: Carnegie stage 1-5. syncytium and penetrate into the endometrial epithelium.

Carnegie stage 4: Attaching blastocyst
5-6 days after fertilization, 0.1-0.2 mm in diameter

This stage is characterized by the attached blastocyst, which corresponds to the onset of implantation. Attachment of the embryo occurs only once the endometrium has entered the secretory phase. At the site of attachment, the trophoblast cells are transformed into a syncytium and penetrate into the endometrial epithelium.

Carnegie stage 5: Implanted but previllous
7-12 days after fertilization, 0.1-0.2 mm in diameter

The blastocyst penetrates into the endometrium. The trophoblast grows rapidly but is previllous, i.e., it does not yet show definite chorionic villi. This stage is sub-divided into 3 stages according to the differentiation status of the trophoblast: solid trophoblast (stage 5a), lacunar trophoblast (5b), and perfusion of lacunae with maternal blood (5c).

Carnegie stage 6: Chorionic villi and primitive streak
13 days after fertilization, 0.2 mm in size

Chorionic villi appear and begin to branch. Trophoblastic lacunae coalesce to form the intervillous space (6a). The extra-embryonic mesoderm arises and the chorionic cavity is formed. The yolk sac is now called the secondary (definitive) yolk sac. The primitive streak appears later during this stage (6b, "stage 6" in Fig. 2).

Carnegie stage 7: Notochordal process
16 days after fertilization, 0.4 mm in length (embryonic disc)

The notochordal process develops in the mesodermal layer rostral to the primitive node. The length of the notochordal process varies from 0.03 to about 0.3 mm. The embryonic mesoderm spreads laterally and rostrally from the primitive streak. The embryonic disc grows cranially and the amniotic cavity expands over the yolk sac.

Carnegie stage 8 : Primitive pit, neuenteric canal
18 days after fertilization, 1.0 mm in CRL (crown-rump length)

This stage is characterized by the formation of the primitive pit, the notochordal canal and the neurenteric canal. Somites are not yet visible (presomitic stage). The embryonic disc is pyriform, tapering caudally. The notochordal canal is marked by the cavity extending from the primitive pit into the notochordal process. The floor of the canal soon disappears to form a passage between the amniotic cavity and the yolk sac (neurenteric canal).

Carnegie stage 9: 1-3 pairs of somites
20 days after fertilization, 1.5 mm in CRL

The neural groove and the first somites appear, and one to three pairs of somites can be observed. The embryonic disc resembles a shoe-sole, with the broad neural plate positioned into the cranial region. The neural groove appears during this stage and subsequently deepens. The paraxial mesoderm becomes segmented to form somites.

Carnegie stage 10: Neural folds begin to fuse, 4-12 pairs of somites
22 days after fertilization, 1.8 mm in CRL

The neural groove deepens and the neural folds begin to fuse to form the neural tube. The fusion of neural folds extends bidirectionally. The optic sulcus and branchial arch 1 (i.e., pharyngeal arch) begin to be visible. The cardiac loop starts to appear.

Carnegie stage 11: Anterior neuropore closes
24 days after fertilization, 2.5-3 mm in CRL

The human embryo now has 13-20 pairs of somites. The anterior neuropore is now closing up. Optic evagination is produced at the optic sulcus and the optic ventricle is continuous with that of the forebrain. The sinus venosus develops in the cardiac loop. The

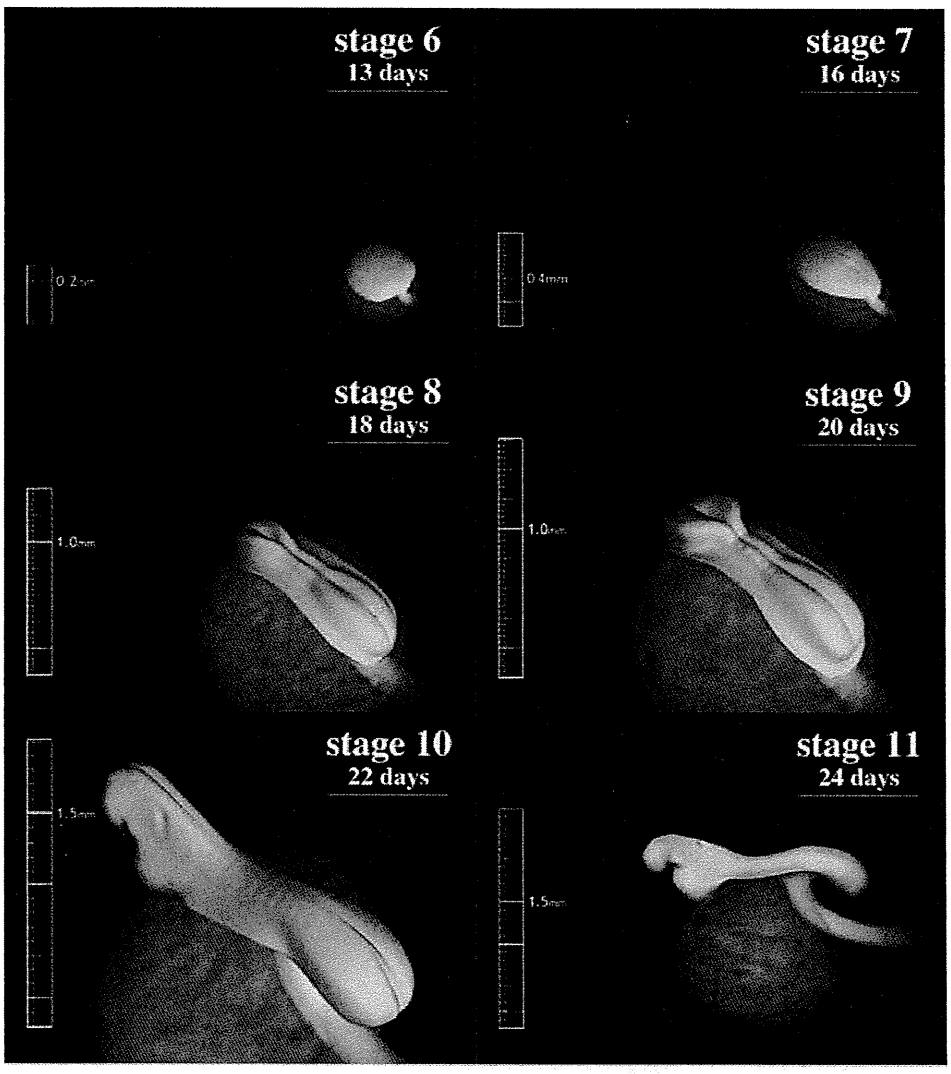

Fig. 4. Computer graphics illustrating human embryonic development: Carnegie stage 6-11. (buccopharyngeal) membrane is ruptured. The otic vesicle is now formed.

Carnegie stage 12: Posterior (caudal) neuropore closes, 3-4 branchial arches, upper limb buds
28 days after fertilization, 4 mm in CRL

The posterior (caudal) neuropore is starting to close or is closed. Three branchial arches are present. Upper limb buds are distinct. The embryo now has 21-29 pairs of somites. The embryonic axis is curved as a result of the rounding out or the folding of the embryo. Internally, the lung bud appears and the interventricular septum has begun its formation in the heart.

Carnegie stage 13: Four limb buds, optic vesicle
32 days after fertilization, 5 mm in CRL

Two upper and two lower limb buds are visible. The optic vesicle can be easily recognized and the lens placode begins to differentiate. The embryo now has more than 30 pairs of

somites, but the number of somites becomes increasingly difficult to determine and is no longer used in staging.

Carnegie stage 14: Lens pit and optic cup
34 days after fertilization, 6 mm in CRL

The lens pit invaginates into the optic cup but is not yet closed. The endolymphatic appendage emerging from the otic vesicle is well defined. The upper limb buds elongate and become tapering. The cephalic and cervical flexures are prominent. Internally, the future cerebral hemispheres and cerebellar plates are visible. The dorsal and ventral pancreatic buds are noticeable. The ureteric bud develops and acquires a metanephrogenic blastemal cap.

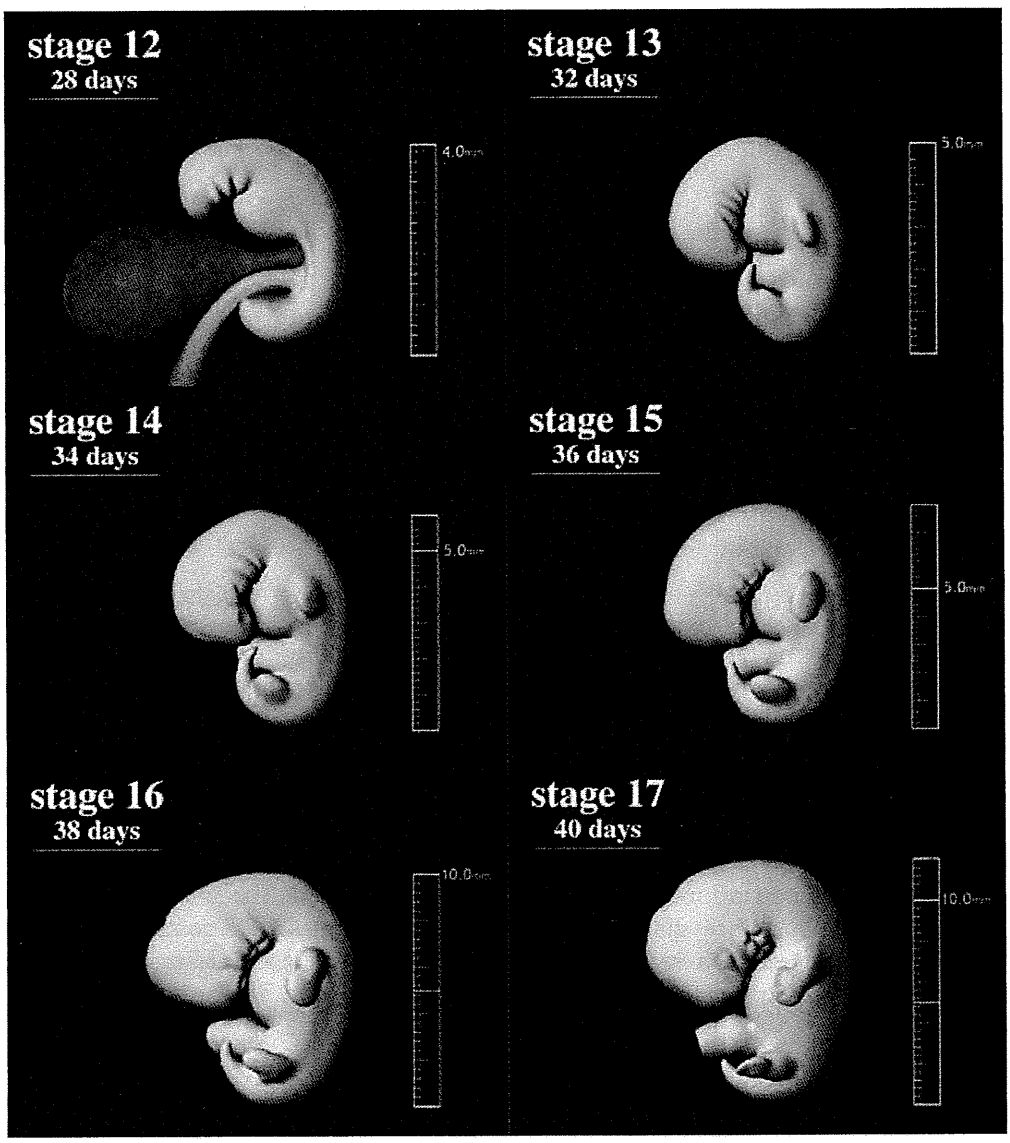

Fig. 5. Computer graphics illustrating human embryonic development: Carnegie stage 12-17.

Carnegie stage 15: Lens vesicles, nasal pit and hand plates
34 days after fertilization, 8 mm in CRL

Lens vesicles are closed and covered by the surface ectoderm. The nasal plate invaginates to form a nasal pit. Auricular hillocks arise. Hand plates are forming. The foramen secundum develops in the heart. Lung buds begin to branch into lobar buds. The primary urogenital sinus is formed.

Carnegie stage 16: Nasal pit faces ventrally, retinal pigment, foot plate
38 days after fertilization, 10 mm in CRL

Nasal pits deepen and come to face ventrally. Retinal pigment is visible externally. The hand plates are now distinct and the foot plate is emerging. The nasolacrimal groove has formed between the frontal and maxillary processes.

Carnegie stage 17: Head relatively larger, nasofrontal groove, finger rays
40 days after fertilization, 11 mm in CRL

The head is relatively larger than previously and the trunk has become straighter. The auricular hillocks and nasofrontal (nasolacrimal) grooves are distinct. The hand plates exhibit definite digital rays, and the foot has acquired a rounded digital plate.

Carnegie stage 18: Elbows, toe rays, eyelid folds, nipples
42 days after fertilization, 13 mm in CRL

The body shape is more cuboidal. Both cervical and lumbar flexures are denoted. The elbows are discernible and interdigital notches appear in the hand plates. Toe rays are observed in the foot plate. Eyelid folds appear. Auricular hillocks are being transformed into specific parts of the external ear. Ossification may begin in some skeletal structures.

Carnegie stage 19: Trunk elongation and straightening
44 days after fertilization, 16 mm in CRL

The trunk begins to elongate and straightens. Eyes and external ears gain definite shape. The eyes are positioned in the front of the face, owing to the growth of the brain. The upper and lower limbs are almost parallel, with pre-axial borders cranially and postaxial borders caudally. Intestines have developed and parts of them can be observed in normal umbilical cord (physiological umbilical hernia).

Carnegie stage 20: Longer upper limb bent at elbow
46 days after fertilization, cranio-rump length: 19 mm in CRL

The angle of cervical flexure becomes small, and the direction of the head goes up. Vascular plexus appears in the superficial tissues of the head. The coiled intestine observed in the umbilical cord has developed. Spontaneous movement begins at this stage. The upper limbs have increased in length and become bent at the elbows and hand joints. Fingers are curving slightly over the chest.

Carnegie stage 21: Fingers longer, hands approach each other
48 days after fertilization, cranio-rump length: 21 mm in CRL

The head becomes round. The superficial vascular plexus of the head has spread and surrounds the head. The tail becomes rudimentary. The hands are slightly flexed at the wrists and nearly come together over the cardiac prominence.

Carnegie stage 22: Eyelids and external ear more developed
50 days after fertilization, 23 mm in CRL

The vascular plexus of the head becomes distinct. The eyelids are thickening and encroaching into the eyes. The tragus and antitragus of the external ear are assuming a more definite form. The position of the external ears becomes higher on the head. The tail has almost disappeared.

Carnegie stage 23: End of embryonic period
52 days after fertilization, 30 mm in CRL

The head has rounded out and the trunk has adopted a more mature shape. The eyelids and ear auricles become definite. The limbs have increased in length and the forearm ascends to or above the level of the shoulder. The vascular plexus is approaching the vertex of the head. The tail has now disappeared. The external genitalia are relatively well developed but sex difference is not yet obvious externally.

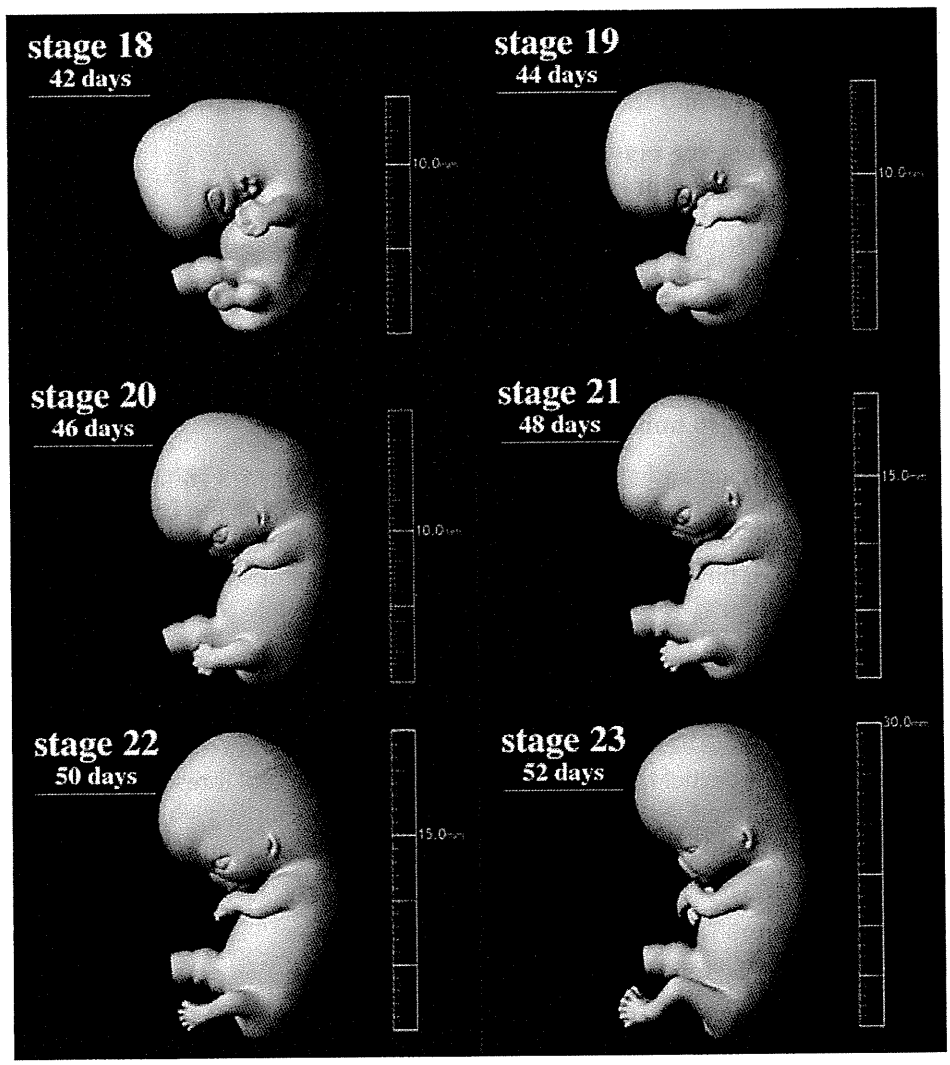

Fig. 6. Computer graphics illustrating human embryonic development: Carnegie stage 18-23.

2.2 The face

Three pharyngeal arches appear at Carnegie stage 12. The 1st pharyngeal gives rise to the maxillary and mandibular prominences (stage 13, Fig. 8), which will then constitute the lateral and caudal boundaries of the stomodeum (i.e., primitive oral cavity), respectively.

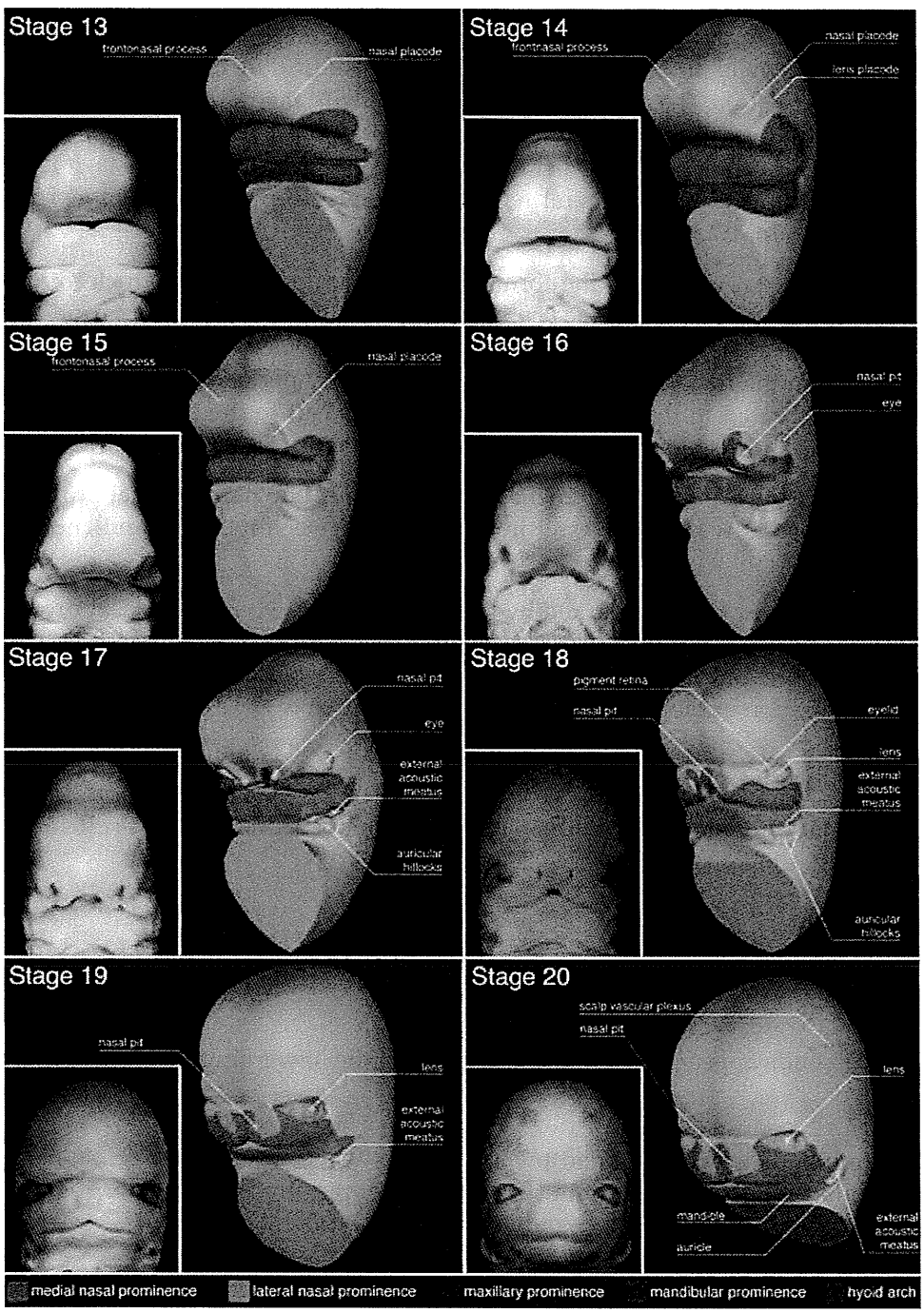

Fig. 7. Embryonic development of the face (stages 13-20).

The side and front of the neck arise from the 2nd pharyngeal arch, also known as the hyoid arch. The frontonasal prominence (FNP) grows to cover the ventral part of the forebrain (stage 13). It will form the forehead (frontal part of the FNP) and the primordial mouth and nose (nasal part of the FNP).

By the end of the 4th developmental week, nasal placodes (thickening of surface ectoderm to become peripheral neural tissue) develop on the frontolateral aspects of the FNP (stage 13). The mesenchyme swells around the nasal placodes resulting in medial and lateral nasal prominences (stage 16). The maxillary prominence will merge with the medial nasal prominences, and cause their fusion. The fused medial nasal prominences will form the midline of the nose and that of the upper lip, as well as the primary palate (stage 16-18). The nasolacrimal groove divides the lateral nasal prominence from the maxillary prominence (observed in stages 16, 17).

The 5th developmental week sees the formation of the primordial ear auricles around the first pharyngeal groove, at the interface between the mandibular prominences and the hyoid arches (stage 16). The auricular hillocks give rise to the auricle while the external acoustic meatus arises from the first pharyngeal groove. At the early period of ear development, the external ears are located in the neck region, and they ascend to the side of the head at the level of the eyes as the development of the mandible (compare Fig. 8 with stage 23 in Fig. 6).

The maxillary and lateral nasal prominences will fuse with the nasolacrimal groove during the 6th developmental week, and result in continuity between the nose and cheek (~stage 18).

The 7th developmental week is marked by the fusion of the two medial nasal prominences with the maxillary and lateral nasal prominences (stage 19~). The merge between the maxillary and medial nasal prominences creates continuity between the upper jaw and lip, and results in partition of the nasal cavity from the oral cavity.

2.3 Upper and lower extremities

The embryonic development of the limbs (O'Rahilly and Gardner, 1975) is illustrated here using computer graphics (Yamada et al., 2006).

Carnegie stage 12

The upper limb buds start to develop.

Carnegie stage 13

The upper limb buds appear in a definite manner, and the lower limb buds start to develop.

Carnegie stage 14

The upper limb buds grow and taper toward the tip, which will later form the hand plate. Innervation and blood supply begin at CS14 in the upper limbs. The development of the lower limb buds is delayed in respect to the upper limb buds.

Carnegie stage 15

The hand plates are distinct in the upper limb buds. In the lower limbs, the rostral half is rounded but the caudal half is tapered. Innervation begins in the lower limb buds.

Carnegie stage 16

Hand plates form a central, carpal part and a digital flange. Lower limb buds form a femoral part, a crural part and foot plate.

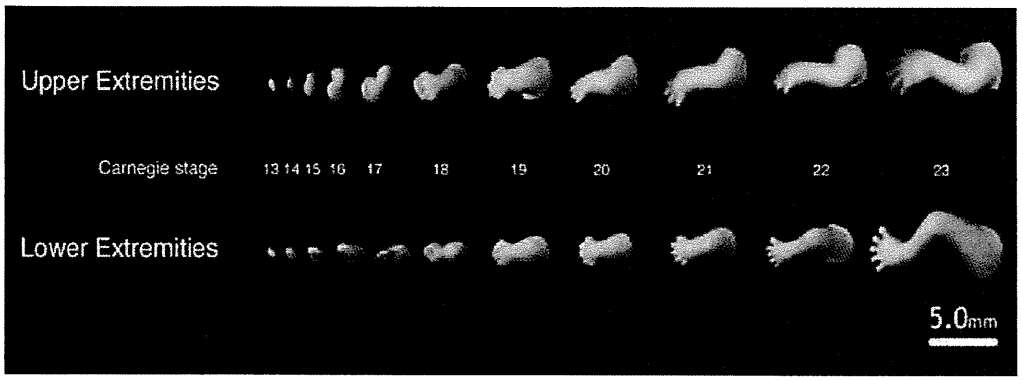

Fig. 8. Embryonic development of upper and lower limbs (CS13-CS23).

Carnegie stage 17

Finger rays appear in the hand plate, and the rim of the hand plate is crenated due to the presence of individual fingers in some advanced specimens. The lower limb buds have increased in size and a rounded digital plate is set off from the crurotarsal region.

Carnegie stage 18

The upper limbs have increased in length and become slightly bent at the elbow. Finger rays are distinct. Toe rays appear but the rim of the foot plate is not yet definitely notched in the lower limb bud.

Carnegie stage 19

The upper limbs rotate medially and seem to hold the chest. Apoptosis occurs in the mesenchymal tissues of interdigital areas, and creates deeper interdigital notches. Toe rays are prominent and interdigital notches appear in the foot plate. Knees and ankles start to appear.

Carnegie stage 20

The upper limbs are bent at the elbow and hand joints, resulting in a pronated position. The lower limbs are also bent at the knee joints. Notches are present between the toe rays in the foot plate.

Carnegie stage 21

Elbows in the upper limbs and knees in the lower limbs now become distinct. Hands cross each other in front of the chest. Fingers are longer and distal phalangeal portions are slightly swollen, indicating the beginning of palmar pads. The feet are also approaching each other.

Carnegie stage 22

Hands extend in front of the body and the fingers of one hand may overlap those of the other. Feet approach each other, but toe digits are still webbed.

Carnegie stage 23

Upper and lower limbs are well formed. They have lengthened and are bent at joints. Fingers get longer and toes are no longer webbed, all digits are now separate and distinct.

3. Conclusion

Large-scale human embryo collections started in the early 20th century and contributed to tremendous progress in human embryology. These compendiums of embryonic specimens are still widely used today, and are exploited through modern technologies such as imaging techniques and computer sciences. Using computer graphics prepared from specimens housed at the Kyoto Collection of Human Embryos, here we provided a clear overview of human embryonic development, with a special emphasis on the limbs and the face.

4. Acknowledgments

We are deeply grateful to Ms. Elizabeth Lockett at the National Museum of Health and Medicine, Washington D.C., for providing information on the Carnegie Collection; Dr. Sumiko Kimura for assistance and guidance in the experiments; Ms. Chigako Uwabe at the Congenital Anomaly Research Center at Kyoto University Graduate School of Medicine for technical assistance; Prof. Michihiko Minoh, Dr. Takuya Funatomi, Dr. Tamaki Motoki, Ms. Mikiko Takahashi, and Mr. Yutaka Minekura at the Academic Center for Computing and Media Studies at Kyoto University, for generating the computer graphics of human embryos; and Prof. Kohei Shiota, Vice President of Kyoto University for his support and guidance on the project. Part of this research was financially supported by Grants #228073, #238058, #21790180 and #22591199 from the Japan Society for the Promotion of Science (JSPS) and the Japan Science and Technology (JST) institute for Bioinformatics Research and Development (BIRD). The studies presented in this chapter were approved by the Medical Ethics Committee at Kyoto University Graduate School of Medicine (Kyoto, Japan).

5. References

Brown, D. D. 1987. The Department of Embryology of the Carnegie Institution of Washington. *BioEssays : news and reviews in molecular, cellular and developmental biology,* 6, 92-6.

Haishi, T., Uematsu, T., Matsuda, Y. & Kose, K. 2001. Development of a 1.0 T MR microscope using a Nd-Fe-B permanent magnet. *Magnetic resonance imaging.* 19, 875-80.

Hirose, A., Nakashima, T., Yamada, S., Uwabe, C., Kose, K. & Takakuwa, T. 2012. Embryonic liver morphology and morphometry by magnetic resonance microscopic imaging. *Anatomical record: advances in integrative anatomy and evolutionary biology.* 2011. 295, 51-59.

Hopwood, N. 2007. A history of normal plates, tables and stages in vertebrate embryology. *The International journal of developmental biology,* 51, 1-26.

Iffy, L., Shepard, T. H., Jakobovits, A., Lemire, R. J. & Kerner, P. 1967. The rate of growth in young human embryos of Streeter's horizons. 13 to 23. *Acta anatomica,* 66, 178-86.

Jirásek, J. E. 1971. *Development of the genital system and male pseudohermaphroditism,* Baltimore, Johns Hopkins Press.

Kameda, T., Yamada, S., Uwabe, C., Shiota, K. & Suganuma, N. 2012. Digitization of clinical and epidemiological data from the Kyoto Collection of Human Embryos: maternal risk factors and embryonic malformations. *Congenital Anomalies.* doi: 10.1111/j.1741-4520.2011.00349.x

Mall, F. P. 1914. On stages in the development of human embryos from 2 to 25mm long. *ANATOMISCHER ANZEIGER,* 46, 78-84.

Matsuda, Y., Ono, S., Otake, Y., Handa, S., Kose, K., Haishi, T., Yamada, S., Uwabe, C. & Shiota, K. 2007. Imaging of a large collection of human embryo using a super-parallel MR microscope. *Magnetic resonance in medical sciences: MRMS: an official journal of Japan Society of Magnetic Resonance in Medicine.* 6, 139-46.

Matsuda, Y., Utsuzawa, S., Kurimoto, T., Haishi, T., Yamazaki, Y., Kose, K., Anno, I. & Marutani, M. 2003. Super-parallel MR microscope. *Magnetic resonance in medicine : official journal of the Society of Magnetic Resonance in Medicine / Society of Magnetic Resonance in Medicine.* 50, 183-9.

Matsunaga, E. & Shiota, K. 1977. Holoprosencephaly in human embryos: epidemiologic studies of 150 cases. *Teratology,* 16, 261-72.

Nishimura, H. 1974. Detection of early developmental anomalies in human abortuses. *In:* Gianantonio, C. A., Berri, G. G. (ed.) *Pediatria XIV.* Buenos Aires: Editorial Medica Panamericana.

Nishimura, H. 1975. Prenatal versus postnatal malformations based on the Japanese experience on induced abortions in the human being. . *In:* BLANDEU, R. (ed.) *Aging Gamates.* Basel: S. Karger AG.

Nishimura, H. 1983. Introduction. *In:* Nishimura, H. (ed.) *Atlas of Human Prenatal Histology.* Tokyo: Igaku-shoin.

Nishimura, H., Takano, K., Tanimura, T. & Yasuda, M. 1968. Normal and abnormal development of human embryos: first report of the analysis of 1,213 intact embryos. *Teratology,* 1, 281-90.

Nishimura, H., Tanimura, T., Semba, R. & Uwabe, C. 1974. Normal development of early human embryos: observation of 90 specimens at Carnegie stages 7 to 13. *Teratology,* 10, 1-5.

O'Rahilly, R. 1988. One Hundred Years of Human Embryology. *In:* KALTER, H. (ed.) *Issues and Reviews in Terratology* New York: Plenum Press.

O'Rahilly, R. & Gardner, E. 1975. The timing and sequence of events in the development of the limbs in the human embryo. *Anatomy and embryology.* 148, 1-23.

O'Rahilly, R. & Müller, F. 1987. *Developmental stages in human embryos: including a revision of Streeter's "horizons" and a survey of the Carnegie Collection.,* Washington, DC, Carnegie Institution of Washington Publication.

Olivier, G. & Pineau, H. 1962. Horizons de Streeter et age embryonnaire. *Bulletin de l'Association des anatomistes.* 47, 573-576.

Shiota, K. 1991. Development and intrauterine fate of normal and abnormal human conceptuses. *Congenit Anom Kyoto,* 31, 67-80.

Streeter, G. L. 1942. Developmental horizons in human embryos. Description of age group XI, 13 to 20 somites, and age group XII, 21 to 29 somites. *Carnegie Institution of Washington publication 541, Contributions to Embryology,* 30, 211-245.

Streeter, G. L. 1945. Developmental horizons in human embryos. Description of age group XIII, embryos about 4 or 5 millimeters long, abd age group XIV, period of indentation of the lens vesicle. *Carnegie Institution of Washington publication 557, Contributions to Embryology,* 31, 27-63.

Streeter, G. L. 1948. Developmental horizons in human embryos. Description of age groups XV, XVI, XVII, and XVIII, being the third issue of a survey of the Carnegie Collection. *Carnegie Institution of Washington publication 575, Contributions to Embryology,* 32, 133-203.

Streeter, G. L. 1951. Developmental horizons in human embryos. Description of age groups XIX, XX, XXI, XXII, and XXIII, being the fifth issue of a survey of the Carnegie Collection (prepared for publication by C. H. Heuser and G. W. Corner). *Carnegie Institution of Washington publication 592, Contributions to Embryology,* 34, 165-196.

Yamada, S. 2006. Embryonic holoprosencephaly: pathology and phenotypic variability. *Congenital anomalies,* 46, 164-71.

Yamada, S., Samtani, R. R., Lee, E. S., Lockett, E., Uwabe, C., Shiota, K., Anderson, S. A. & Lo, C. W. 2010. Developmental atlas of the early first trimester human embryo. *Developmental dynamics : an official publication of the American Association of Anatomists,* 239, 1585-95.

Yamada, S., Uwabe, C., Fujii, S. & Shiota, K. 2004. Phenotypic variability in human embryonic holoprosencephaly in the Kyoto Collection. *Birth defects research. Part A, Clinical and molecular teratology.* 70, 495-508.

Yamada, S., Uwabe, C., Nakatsu-Komatsu, T., Minekura, Y., Iwakura, M., Motoki, T., Nishimiya, K., Iiyama, M., Kakusho, K., Minoh, M., Mizuta, S., Matsuda, T., Matsuda, Y., Haishi, T., Kose, K., Fujii, S. & Shiota, K. 2006. Graphic and movie illustrations of human prenatal development and their application to embryological education based on the human embryo specimens in the Kyoto collection. *Developmental dynamics : an official publication of the American Association of Anatomists,* 235, 468-77.

Yoneyama, A., Yamada, S. & Takeda, T. 2011. Fine Biomedical Imaging Using X-Ray Phase-Sensitive Technique. *In:* Gargiulo, D. G., Mcewan, A. (ed.) *Advanced Biomedical Engineering.* InTech. p107-128.

7

Developmental Anatomy of the Human Embryo – 3D-Imaging and Analytical Techniques

Shigehito Yamada[1], Takashi Nakashima[2], Ayumi Hirose[2], Akio Yoneyama[3], Tohoru Takeda[4] and Tetsuya Takakuwa[2]
[1]*Congenital Anomaly Research Center, Kyoto University,*
[2]*Human Health Science, Kyoto University,*
[3]*Central Research Laboratory, Hitachi Ltd.,*
[4]*Allied Health Sciences, Kitasato University,*
Japan

1. Introduction

Prenatal or antenatal development is a process during which the human embryo undergoes complex morphogenetic changes. To understand and characterize the dynamic events underlying human ontogenesis, it is useful to visualize embryonic structures in three-dimensions (3D). Classically, solid reconstruction and fine drawing have been the primary approaches used to model the architecture of the embryonic body. The most impressive wax models of staged human embryos are housed at the Carnegie Institution of Washington DC in the Human Developmental Anatomy Center (see Fig. 1 in Chapter 1). The wax plate technique of reconstruction was first introduced to human embryology by Gustav Born (1883), and later modified in the Carnegie Laboratory in Baltimore by Osborne O. Heard and his colleagues (Heard, 1951, Heard, 1953, Heard, 1957). The procedure involves embedding of human embryos in paraffin wax, followed by serial sectioning and histological staining. Wax plates were cut faithfully as the enlarged image of each section, and the wax plates were piled up for making the 3D embryonic structures. These reconstructed models allowed for the production of accurate drawings of human embryos, some of the most notable being those of James F. Didusch, a medical artist who added valuable information to the understanding of human prenatal development (O'Rahilly, 1988). However, both solid reconstruction and fine drawings used in classical embryology are time-consuming and require specific and rare skills.

In the past decades, the visualization of biological structures has been significantly facilitated by computer-assisted techniques, allowing for the three-dimensional reconstruction of human embryos from section images and offering the unique ability to manipulate reconstructed images. The difficulties that have hindered efforts in 3D reconstruction using two-dimensional image stacks revolve around the issues of section registration and distortion. A solution has come about with the advent of Episcopic Fluorescence Image Capture (EFIC), a novel imaging modality for the generation of high-

resolution 3D reconstruction (Weninger and Mohun, 2002; see 2.2.1). With EFIC imaging, tissue autofluorescence is used to image the block face prior to cutting each section. Although the samples have been sliced and lost during the procedure, the optical resolution of EFIC was reported to reach approximately 5-6 μm (Yamada et al., 2010) and EFIC enables us to obtain 3D images with high-resolution comparable to the images of histological serial sections. On the other hand, remarkable progress has been made in nondestructive imaging technologies such as magnetic resonance (MR) imaging. MR imaging was originally developed as a non-invasive diagnostic tool in clinical medicine, but recent technological advances has promoted its application to detailed imaging and 3D reconstruction of tiny biological structures such as embryos (Smith, 1999, 2000, 2001, Smith et al., 1994, 1996, 1999; see 2.2.2), reaching a resolution close to 30 μm/pixel. X-ray technology is also widely used for non-destructive imaging of inner structures. Using the characteristics of X-rays as electromagnetic waves, phase-contrast X-ray imaging visualizes the phase-shift of X-ray passing through the samples and reconstructs 2D or 3D images of the samples in combination with computed tomography (Momose et al., 1996, Yoneyama et al., 2011). EFIC, MR microscopy, and phase-contrast X-ray computed tomography (CT) have all been applied to embryology. The imaging modalities are selected on the basis of their destructive vs. non-destructive features, the size of the samples and the desired resolution (Fig. 1).

Morphometrics refers to the quantitative analysis of forms, a concept that encompasses size and shape (Rohlf and Bookstein, 1990). While the qualitative morphological data obtained by classical modalities such as serial sections are not suitable for numerical conversion, the data obtained by 3D-imaging techniques (see 2.2) are easily converted for quantitative analyses. Three-dimensional morphometric analyses of human embryos from the Kyoto Collection are actively underway.

In this chapter, we will describe in detail modern modalities currently used for human embryo imaging and their applications to developmental anatomy.

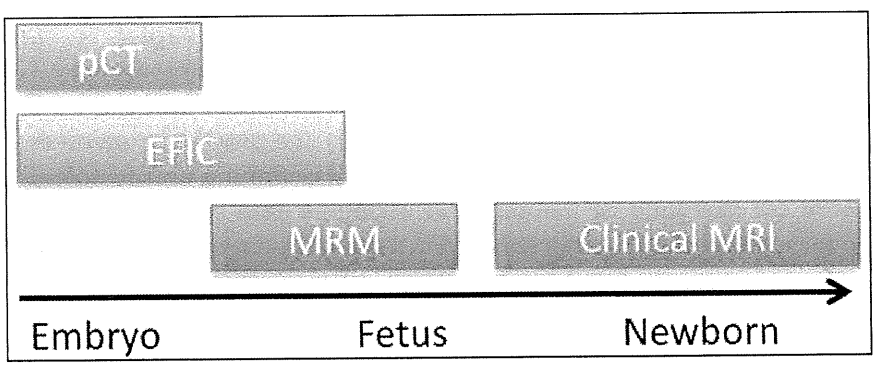

Fig. 1. Relationship between sample size and imaging techniques. pCT: phase-contrast X-ray computed tomography, EFIC: episcopic fluorescence image capture, MRM: magnetic resonance microscopy, Clinical MRI: magnetic resonance imaging for routine clinical use.

2. Imaging modalities for three-dimensional analyses

2.1 Digital reconstruction from serial sections

Classical reconstruction methods based on wax models have been described earlier. In "modern" computer-assisted reconstruction, stained histological sections are digitized using

a digital camera equipped with a normal bright-field illumination. The color images of the serial sections (Fig. 2A) are then saved as TIFF files and a 3D reconstruction can be obtained using DeltaViewer (see 5. Appendix), a software designed to perform automated alignment and 3D reconstruction from serial sections. Once aligned, the images are then segmented using painting softwares (Fig. 2B) and 3D images are obtained (Fig. 2C). Further details on reconstruction procedures from serial sections can be found in previous publications (Yamada et al., 2007).

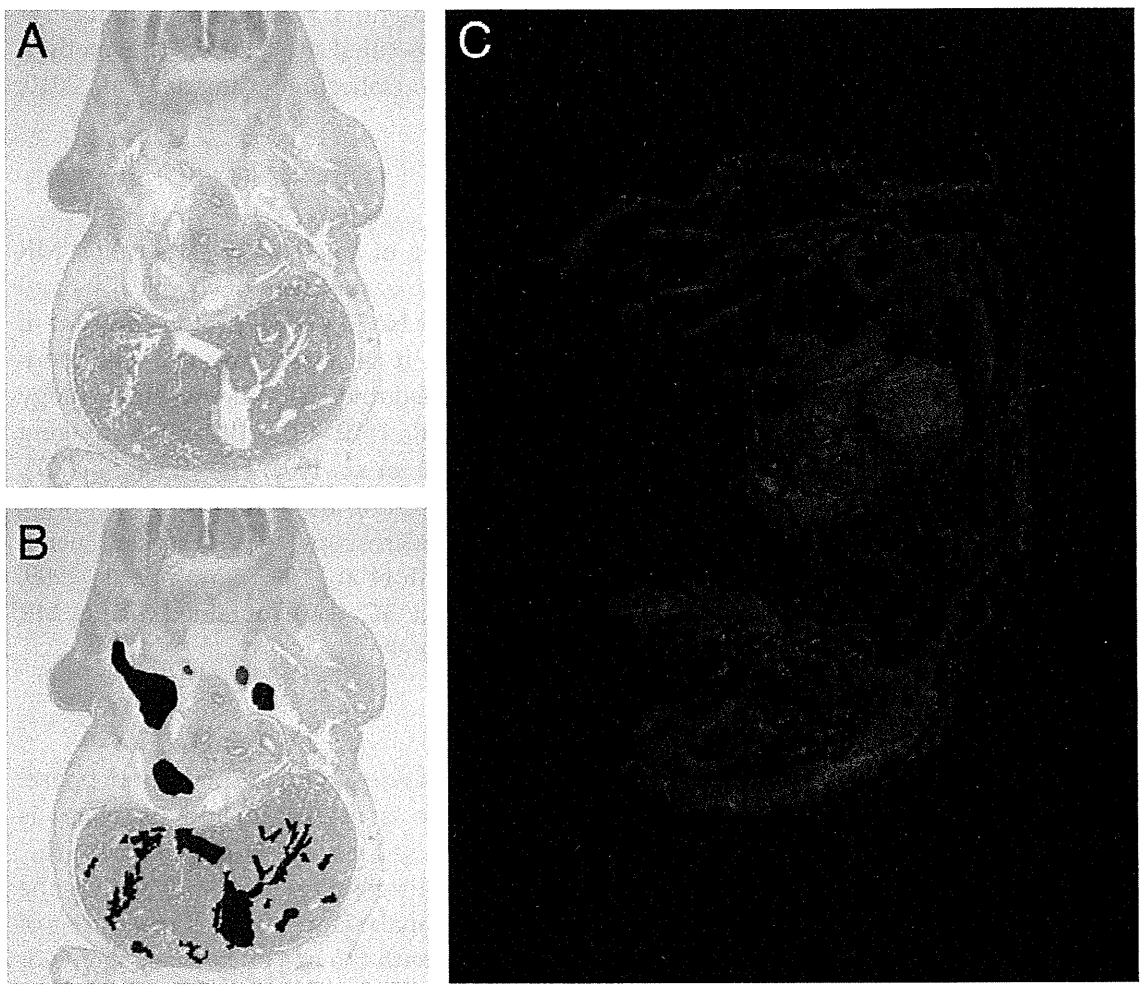

Fig. 2. Three-dimensional reconstruction from serial sections. A,B: Transverse sections of human embryo showing the spinal cord, the root of the upper limb bud, and the liver. The section is digitized (A) and manually segmented (B). C: Three-dimensional reconstruction of the heart and great vessels of human embryo at CS14 using the "DeltaViewer"software.

2.2 3D-imaging

In contrast to serial sections, 3D-imaging allows for rapid 3D rendering such as surface reconstruction and digital resectioning in arbitrary planes. Multiple 3D-imaging modalities have been applied to the human embryos of the Kyoto Collection.

2.2.1 Episcopic fluorescence image capture (EFIC)

Episcopic fluorescence image capture (EFIC) represents a novel 3D-imaging method in human embryology. This imaging technique relies on the embedding of the embryo in paraffin (Weninger and Mohun, 2002), followed by the sectioning of the block using a sliding microtome. Prior to cutting each section, the block face is imaged by capturing tissue autofluorescence. The block is accurately returned to exactly the same photo-position on the microtome, and registered 2D image stacks are automatically generated. EFIC allows for virtual resectioning of the specimen in arbitrary planes (Rosenthal et al., 2004, Weninger et al., 2006), and rapid high-resolution 3D reconstructions (Rosenthal et al., 2004). This method was applied to staged human embryos housed at the Kyoto Collection (Yamada et al., 2010; see Figure 3A).

2.2.2 Magnetic resonance microscopy

Magnetic resonance (MR) imaging applied to the scanning of small samples is called MR microscopy. MR microscopy is a very powerful tool for 3D measurement of chemically-fixed human embryos because of the large amounts of mobile or NMR visible protons present in the formalin preservation fluid (Matsuda et al., 2007). It is a non-invasive and non-destructive imaging process, and has been previously applied to developmental embryology in a number of animal models (Bone et al., 1986, Smith et al., 1992, 1994, 1996). MR imaging offers highly beneficial features (Effmann et al., 1988, Smith et al., 1992, Haishi et al., 2001), reaching a resolution of 40 μm/pixel or higher when scanning the samples for extended periods of time. Imaging of human embryos by MR microscopy was described using superconducting magnets ranging from 1.0T to 9.4T (Smith et al., 1996, Smith et al., 1999, Haishi et al., 2001). The images shown in Fig. 3B and 3C were obtained using MR microscopes equipped with 7T and 2.34T magnets, respectively.

2.2.3 Phase-contrast X-ray computed tomography

X-rays are electromagnetic waves, and are thus, characterized by amplitude and phase. When an X-ray passes through a sample, its amplitude is decreased and its phase is shifted. Conventional X-ray imaging (radiography) is based on absorption-contrast (i.e. amplitude imaging) and represents the mass-density distribution of X-ray inside the sample. Its sensitivity is insufficient to perform detailed analysis of samples consisting of biological soft tissues such as embryos, unless combined with the use of contrast agents or applying higher X-ray doses. Exploiting the phase information of X-rays is a solution. The sensitivity of the phase shift for light elements such as hydrogen, carbon, nitrogen, and oxygen is about 1000 times larger than that of absorption (Momose and Fukuda, 1995). To detect a phase-shift, it is essential to convert the phase shift into a change in X-ray intensity as X-ray intensities are classically measured using current-detecting devices. Conversion methods such as interferometry and diffractometry are used for the generation of 2D and 3D observations using synchrotron radiation. Devices based on this principle have been developed (Becker and Bonse, 1974, Yoneyama et al., 2004), and an image of human embryo at CS 17 obtained using a two-crystal X-ray interferometer (Yoneyama et al., 2011) is featured in Fig. 3D.

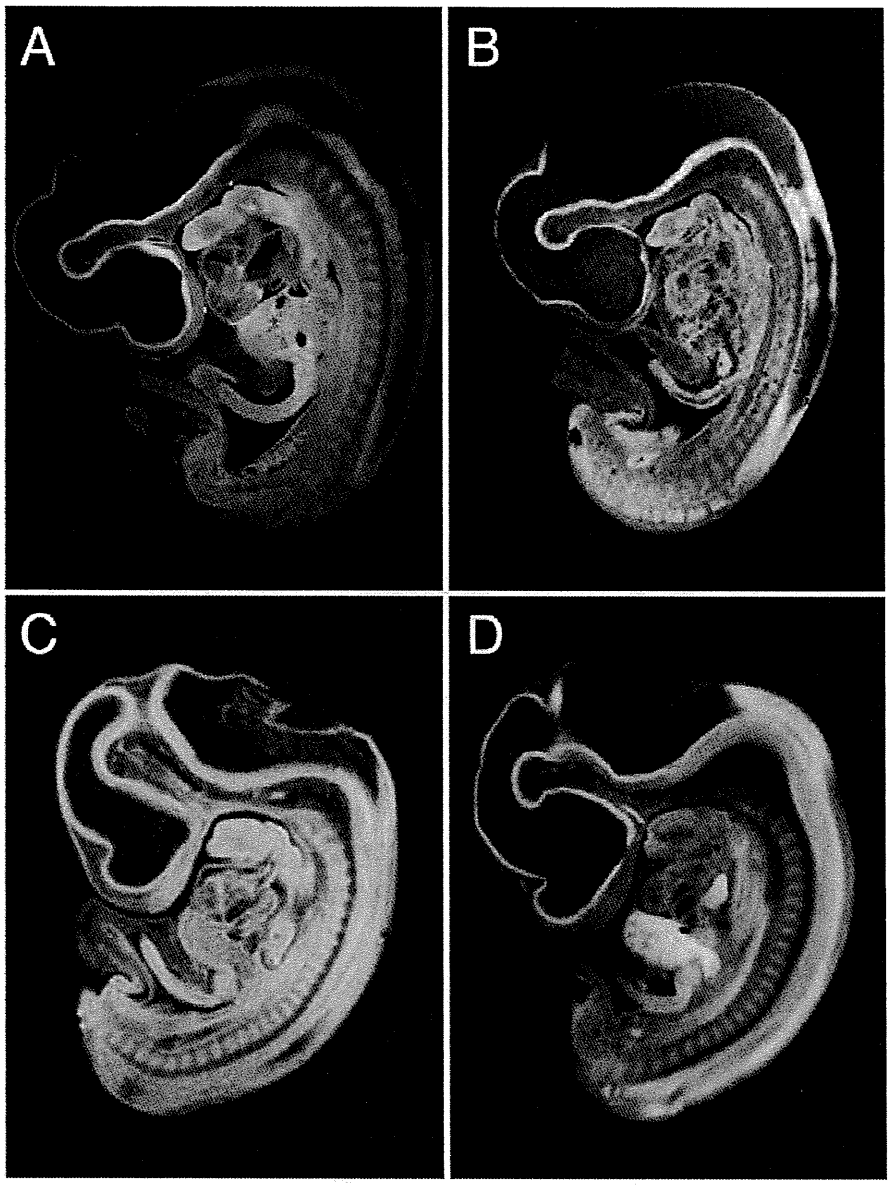

Fig. 3. Images of human embryos obtained using various imaging modalities. CS16 embryo imaging using EFIC (A) and 7T-MRI (B), CS17 embryo imaging using 2.34T MRI (C) and phase-contrast x-ray CT at 17.8keV X-ray energy (D).

3. Analyses of developmental anatomy using 3D-imaging

3.1 MR microscopy project at the Kyoto collection of human embryos

The Kyoto collection counts approximately 45,000 human embryos, and contains historical specimens housed at the Congenital Anomaly Research Center of Kyoto University (Nishimura et al., 1968, Nishimura, 1975, Shiota, 1991, Yamada et al., 2004). Most specimens were obtained from pregnancies terminated during the first trimester due to socioeconomic reasons as legally permitted under the Maternity Protection Law of Japan. Some of the

specimens (~20%) are undamaged, well-preserved embryos. When the aborted materials were brought to the laboratory, the embryos were measured, examined, and staged according to the criteria of O'Rahilly and Müller (1987). Further information on the Kyoto Collection of Human Embryos can be found in Chapter 1. In 1999, Kyoto University and the University of Tsukuba initiated a collaborative project aiming to acquire 3D MR microscopic images of thousands of human embryos using a super-parallel MR microscope operated at 2.34T (Matsuda et al., 2003, 2007, Yamada et al., 2006, Shiota et al., 2007). During the course of the project, over 1,200 human embryos were scanned. Further information on the data generated can be found on the web (http://mrlab.frsc.tsukuba.ac.jp/human_embryos/).

3.2 Flow chart: from MR image acquisition to 3D image reconstruction

Approximately 1,200 well-preserved human embryos diagnosed as externally normal at CS13 to CS23 were selected for MR microscopic imaging (Fig. 4A)(Matsuda et al., 2003, 2007,

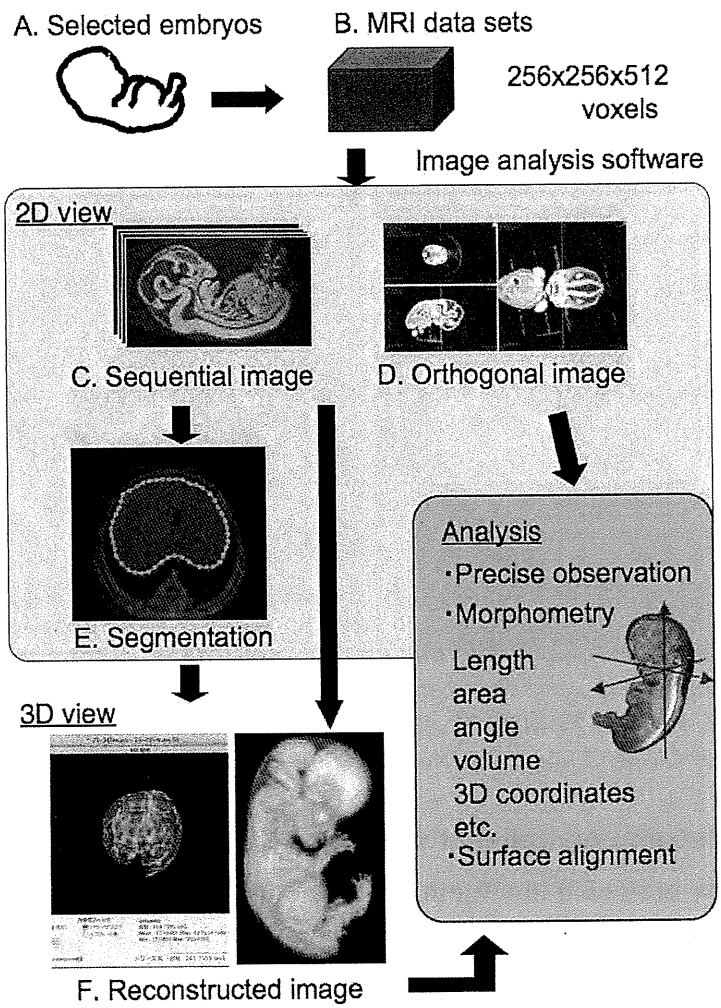

Fig. 4. Flow chart: from MR image acquisition to 3D image reconstruction

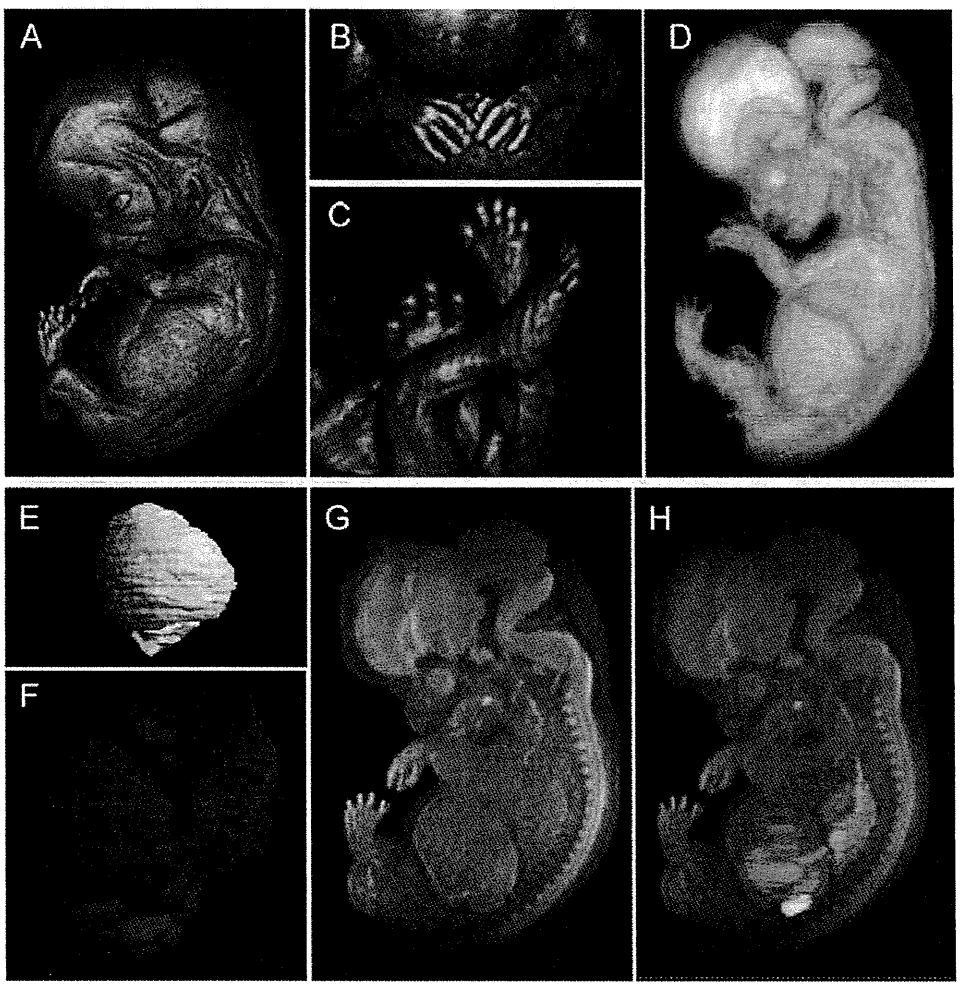

Fig. 5. Samples of 3D reconstructed images. A) 3D images of whole embryo at CS 23 using volume rendering algorithm (Osirix) to observe surfaces. B,C) Magnification of upper and lower extremities, demonstrating fine and detailed reconstruction of embryonic morphology. D) When modifying the volume-rendering settings, both external and internal embryonic structures can be observed. E) 3D-reconstruction of the embryonic liver at CS 23 obtained from segmentation of 2D sequential images. F) Liver (green), lung (blue), heart (red), kidney (yellow), and adrenal glands (purple) were segmented from 2D sequential images and reconstructed in 3D. G) 3D-reconstruction using Maximum intensity projection (MIP) tool (Osirix) in order to generate both surface and internal imaging perspectives. H) Organ images shown in F were overlaid with MIP images shown in G.

Yamada et al., 2006, Shiota et al., 2007). The 3D MR image datasets for each embryo were initially obtained from 256x256x512 voxels (Fig. 4B). Each dataset was subsequently converted into two-dimensional (2D) image stacks (Fig. 4C), which were then digitally resectioned following predefined planes (Fig. 4D). Organs of interest were segmented in series of 2D images (Fig. 4E) and the 3D architectures were computationally reconstructed (Fig. 4F). Images obtained can be freely rotated on the screen, and 3D shapes are easily recognizable and their spatial relationships rapidly determined. The obtained 2D and 3D images obtained can be subjected to further analysis.

3.3 Further processing of reconstructed 3D images using computer software

Recent advances in computer technology have significantly facilitated image rendering on personal computers. A number of algorithms have been developed resulting in multiple 3D reconstruction softwares, many of which are available as open-source. The most popular softwares are summarized in the Appendix section of this chapter. Samples of reconstructed images using such rendering algorithms are represented in Fig. 5.

3.3.1 Imaging using volume rendering techniques (Fig. 5A-D)

Volume rendering techniques are utilized to reconstruct whole embryo images. The display and comparative analysis of 3D images at various developmental stages enables a clearer understanding of embryonic morphogenesis.

Carnegie stages are primarily defined based on external structural features, e.g. cranial facial morphogenesis including eye, nose, pharyngeal arches related organs, posture of the whole embryo, finger and toe development (O'Rahilly and Müller, 1987). The external morphologies obtained by volume rendering have enough quality to determine the developmental stages of the embryos. Because these external morphologies are strictly preserved in this method, the judgment of the staging was identical with that used with original embryo specimens.

3.3.2 Three-dimensional reconstruction from segmentation of 2D sequential images (Fig. 5E, 5F)

Regions of interest (ROI) were segmented from 2D images and then reconstructed using ROI and Osirix reconstruction module. Multiple organs can be individually segmented and combined into 3D images, showing a spatial relationship clearly between adjacent organs. One limitation to 3D image rendering is the lack of information on color and touch sense e.g. pigmentation of the retina, color of superficial arteries or internal organs such as the heart. When modifying the volume rendering settings, external and internal embryonic structures can be observed simultaneously.

3.3.3 Imaging using maximum intensity projection (MIP) method (Fig. 5G, 5H)

Information on both external and internal structures can be acquired using the MIP method (Nakashima et al., 2011). Three-dimensional images obtained by MIP can be superimposed with 3D reconstruction obtained from segmented images, thus creating a see-through effect with internal organs visible from the outside.

3.4 Analysis on 3D reconstructed images

3.4.1 Three-dimensional morphological observation

Three-dimensional reconstruction offers a number of advantages. For instance, the resulting image is amenable to comprehensive examination as the image can be freely rotated on the screen, 3D shapes are easily recognizable and spatial relationships between adjacent organs or tissues become obvious. In Fig. 6, 3D reconstructed images of the embryonic liver (CS18)